Shap. Mem. Superelasticity (2018) 4:112–120
https://doi.org/10.1007/s40830-017-0139-7

SPECIAL ISSUE: A TRIBUTE TO PROF. SHUICHI MIYAZAKI – FROM FUNDAMENTALS TO APPLICATIONS, INVITED PAPER

Fabrication of SLM NiTi Shape Memory Alloy via Repetitive Laser Scanning

Zhong Xun Khoo[1] · Yong Liu[2] · Zhi Hong Low[2] · Jia An[3] · Chee Kai Chua[3] · Kah Fai Leong[1]

Published online: 5 January 2018

Abstract Additive manufacturing has the potential to overcome the poor machinability of NiTi shape-memory alloy in fabricating smart structures of complex geometry. In recent years, a number of research activities on selective laser melting (SLM) of NiTi have been carried out to explore the optimal parameters for producing SLM NiTi with the desired phase transformation characteristics and shape-memory properties. Different effects of energy density and processing parameters on the properties of SLM NiTi were reported. In this research, a new approach—repetitive laser scanning—is introduced to meet these objectives as well. The results suggested that the laser absorptivity and heat conductivity of materials before and after the first scan significantly influence the final properties of SLM NiTi. With carefully controlled repetitive scanning process, the fabricated samples have demonstrated shape-memory effect of as high as 5.11% (with an average value of 4.61%) and exhibited comparable transformation characteristics as the NiTi powder used. These results suggest the potential for fabricating complex NiTi structures with similar properties to that of the conventionally produced NiTi parts.

✉ Yong Liu
mliuy@ntu.edu.sg

[1] School of Mechanical and Aerospace Engineering, Institute for Sports Research, Nanyang Technological University, Singapore, Singapore

[2] School of Mechanical and Aerospace Engineering, Nanyang Technological University, Singapore, Singapore

[3] School of Mechanical and Aerospace Engineering, Singapore Centre for 3D Printing, Nanyang Technological University, Singapore, Singapore

Keywords 3D printing · 4D printing · Additive manufacturing · Selective laser melting · NiTi · Shape-memory alloy

Introduction

Shape memory alloys (SMAs) are widely used due to their superior functional properties and high actuation energy density [1–4]. The most popular SMA is NiTi. However, NiTi SMA has a poor machinability associated with its unconventional deformation mechanisms (detwinning and stress-induced martensitic transformation). The majority of the conventionally produced NiTi parts have simple geometries, and the full potential of NiTi is critically limited by the manufacturing processes [2, 5–7]. Therefore, Selective Laser Melting (SLM) is proposed in recent years to overcome these existing challenges of producing NiTi components with complex geometry [1, 3, 5, 7–22].

Among the studies on SLM of NiTi, Meier et al. [5] and Haberland et al. [7] stated that the minimum energy density required for producing dense SLM NiTi was 85 and 200 J/mm^3, respectively. However, with increasing energy density above the optimal magnitude, three adverse effects were reported. First, Bormann et al. [14] and Haberland et al. [7] noticed an increase in the porosity of the samples up to roughly 10%. Nonetheless, Meier et al. did not observe any effect on the density of SLM NiTi. Second, the impurity pickup increases significantly with energy density beyond the optimum value [7]. Third, the transformation temperatures increase with increasing energy density [7, 8]. This phenomenon is due to Ni evaporation since Ni has a lower evaporation temperature than Ti (the evaporation temperature of Ni is 3186.15 K and the evaporation temperature of Ti is 3560.15 K) [5, 7, 8, 14, 23, 24]. This

occurrence also coincides with the findings of a lower Ni content measured in some of the SLM NiTi samples [5, 14, 16]. Collectively, these three observations illustrate the importance of determining the minimum energy density required in order to produce a dense SLM NiTi material with low impurity content and desired transformation temperatures.

The above-mentioned studies have presented the possibility of controlling the chemical composition and transformation temperatures of SLM NiTi by varying the energy density alone. However, the research by Dadbakhsh et al. [3] and Speirs et al. [16] shown otherwise. Although similar magnitudes of energy density were adopted, Dadbakhsh et al. reported that the variations in SLM process parameters have a significant influence on the transformation temperatures [3]. Speirs et al. noticed that the atmospheric condition such as the oxygen content had a strong effect on the transformation characteristics [16].

Nevertheless, the findings reported on the effects of energy density and processing parameters offer merely a partial answer to the complex problem encountered in this field of research. This is because energy density is dependent on the laser power, laser scanning speed, hatch distance, powder layer thickness, etc. The variation of these parameters will alter the energy density. Hence, there is no clear distinction between the effects of energy density and process parameters. This may also explain why different researchers have observed different phenomena. For instance, Zhang et al. reported the negligible influence of laser scanning speed on the transformation temperatures [10]. This contradicts the findings of Bormann et al. [14] and Speirs et al. [16]. Bormann et al. noticed that the amount of Ni loss and the differences in transformation temperatures are dependent on the exposure time or scanning speed [14]. Speirs et al. stated that the martensitic transformation start (M_s) temperature reduces with the increase in scanning speed [16]. Undeniably, more studies are needed to verify these conflicting results. Although energy density can stay constant while the scanning speed varies, it is only possible to achieve by varying the other parameters as well. Thus, the observations on the effect of scanning speed, given a constant energy density, may not be entirely correct.

Besides, the SLM process was also found to produce strong textures in SLM NiTi samples by orientating the grains towards a specific direction [14, 17]. The grains orientation has led to different shape-memory responses and mechanical properties exhibited. Furthermore, the samples can demonstrate different degrees of shape recovery per unit change in temperature as well. Most of the SLM NiTi samples produced have exhibited sharp transformation peaks [1, 3, 5, 7, 8, 13, 17]. However, Clare et al. have fabricated samples with a much gradual phase transformation than the conventional NiTi parts [15]. This allows the fraction of each phase present to be more manageable and gives rise to an easier control over the material properties. In addition, some researchers have demonstrated the presence of shape memory effect (SME) upon subjecting their SLM NiTi samples to compressive loadings [1, 3, 7, 13, 17]. Nonetheless, there is limited report on the shape-memory properties under tensile load [22], even though it is an important test to conduct.

In this research of fabricating NiTi via the SLM process, the objective is to produce NiTi SMA with minimal porosity, low impurity, optimal mechanical property, controllable transformation characteristics and optimal SME. These objectives are met by (1) introducing a new approach—repetitive scanning—and (2) through the consideration of laser absorptivity and heat transfer that occurs during the fabrication process. The produced samples were characterised and they exhibited a promising result of an average value of 4.61% shape recovery strain under tension mode.

Experimental Procedure

Material

The pre-alloyed NiTi powder (Metal Powders and Materials LLP) used ranges mainly from 20 to 50 µm. Its average chemical composition was determined by two methods: (1) by using the empirical relationship between the chemical composition of NiTi and its M_s temperature [25]; and (2) by using energy-dispersive X-ray spectroscopy (EDX) (Oxford Instruments, Inca x-stream) on the NiTi powder. The phase transformation temperatures (martensitic transformation start (M_s) and finish (M_f) temperatures, austenitic transformation start (A_s) and finish (A_f) temperatures) were obtained by performing differential scanning calorimetry (DSC) testing on the powder particles. The average atomic percentage of the material is approximated to be about 50.16% Ni and 49.84% Ti.

Material Processing

A custom-made SLM equipment (Precision Laser Solutions, Singapore) was used to produce the single-layered NiTi samples. A thick layer of powder was deposited on top of an aluminium base plate, followed by directing the laser onto the powder bed. However, only the top layer will be melted and solidified, leaving a layer of powder between the samples and the base plate. This fabrication method helps prevent contamination due to the possible reaction with aluminium. Moreover, it makes the removal of the samples much easier and convenient as well.

Impurity pickup by the samples was minimised by purging the fabrication chamber with argon gas (purity more than 99.9995%). The purging cycle was repeated several times till the oxygen content reduced to less than 0.1%. The chamber was then maintained at a high pressure with argon gas to prevent atmospheric air from entering during the scanning process.

The samples were fabricated by introducing two-step scanning. During the first scan (S1), various magnitudes of laser power from 15 to 60 W were used. During the second scan (S2), the laser was directed onto the prior solidified layer with a constant laser power of 60 W. The corresponding linear energy density (E) was determined from Eq. (1) [26].

$$E = \frac{P}{v}, \tag{1}$$

where P refers to the laser power (W) and v denotes the laser scanning speed (mm/s). The scanning speed was maintained constant at 3600 mm/s during both scans and the magnitudes of E range from 4.17 to 16.67 J/m.

For the optimisation process, square samples were fabricated by scanning an area with dimensions of 5 mm by 5 mm. Long strip samples were produced by scanning a 5 mm by 78 mm area for the determination of the shape-memory responses. The long strip samples were wire cut to 3.5-mm width prior to the testing. Following, the cut samples were polished to remove the burrs, surface unevenness and excess powder particles. The samples were then heated up above the A_f temperature and cooled below the M_f temperature. The heating process ensured that the detwinned martensite formed during sample preparation was removed and the samples recovered to their initial geometry. The cooling process ensured that the samples were solely in twinned martensitic phase before testing. Four samples were produced for each combination of SLM parameters to check its repeatability.

Material Characterisation

Three properties of SLM NiTi samples were determined: surface morphology, transformation characteristics and stress-free shape-memory response. Scanning electron microscope (SEM) (JEOL, JSM-5600LV) images of the square samples were taken for the observation of their surface morphologies.

The transformation characteristics were determined by using the DSC equipment (TA Instruments, DSC 2920 Modulated DSC). The NiTi powder and SLM samples were subjected to five cycles of cooling and heating processes from a temperature range of −30 °C–120 °C with a ramp rate of 5 °C/min. Only the fifth cycle was presented and utilised for determining the transformation temperatures.

The stress-free shape-memory responses of the fabricated samples were determined under tensile loading. The samples were loaded to a maximum of 8% strain and unloaded to a minimum load of 0.5 N with a strain rate of 0.01%/min at room temperature (Shimadzu, AG–X Plus). The 0.5 N load was then held constant throughout the remaining process. After which, the samples were heated up inside a thermal chamber (Shimadzu, TCE-N300-CE) at a rate of about 2 °C/min and the strain recovery due to SME was recorded. The elongation and thermal expansion of the grips during the loading and heating processes were accounted by calibrating with an alumina plate. During the loading phase, the alumina plate was loaded from 0 to 200 N at room temperature to determine the elongation of the grips. The thermal expansion was determined by loading the plate with a constant force of 0.5 N, followed by heating the grips from room temperature to 120 °C. The plate was assumed to have insignificant deformation during both processes and the data collected were solely due to the elongation and thermal expansion of the grips. A better estimate of the deformation of the samples was obtained by removing these data from the raw results recorded during the respective loading and heating stages.

Results and Discussion

Effect of Repetitive Scanning on Sample's Properties

The SEM images of the square samples fabricated after the first scan (S1) are shown in Fig. 1. These samples were produced using laser power of 15, 25, 40 and 60 W and they are denoted as P15, P25, P40 and P60, respectively. The corresponding magnitudes of linear energy density E adopted were 4.17, 6.94, 11.11 and 16.67 J/m. During the second scan (S2), the laser power was fixed at 60 W with a constant E of 16.67 J/m. The SEM images of the samples subjected to two-step scanning are presented in Fig. 2. These samples are referred as P15–60, P25–60, P40–60 and P60–60.

After the SLM process, the P15–60 samples experienced warpage while P25–60 samples demonstrated smoother and flatter surfaces with minimum defects. Significant formations of porosity (open pores and through holes) and balling effect were observed on P40–60 and P60–60 samples. These occurrences could be attributed to the differences in the laser absorptivity and heat conductivity of materials before and after S1 (NiTi powder and P15 to P60 samples) [27, 28]. Figure 3 illustrates the differences

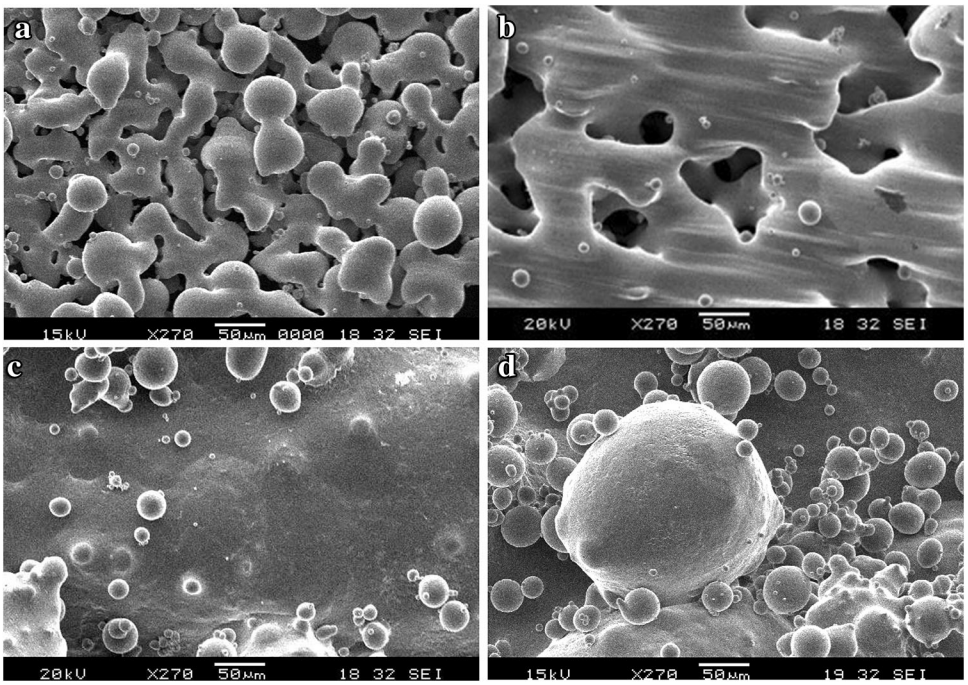

Fig. 1 SEM images of **a** P15, **b** P25, **c** P40 and **d** P60 samples produced after S1. The magnitudes of E used were 4.17, 6.94, 11.11 and 16.67 J/m, respectively

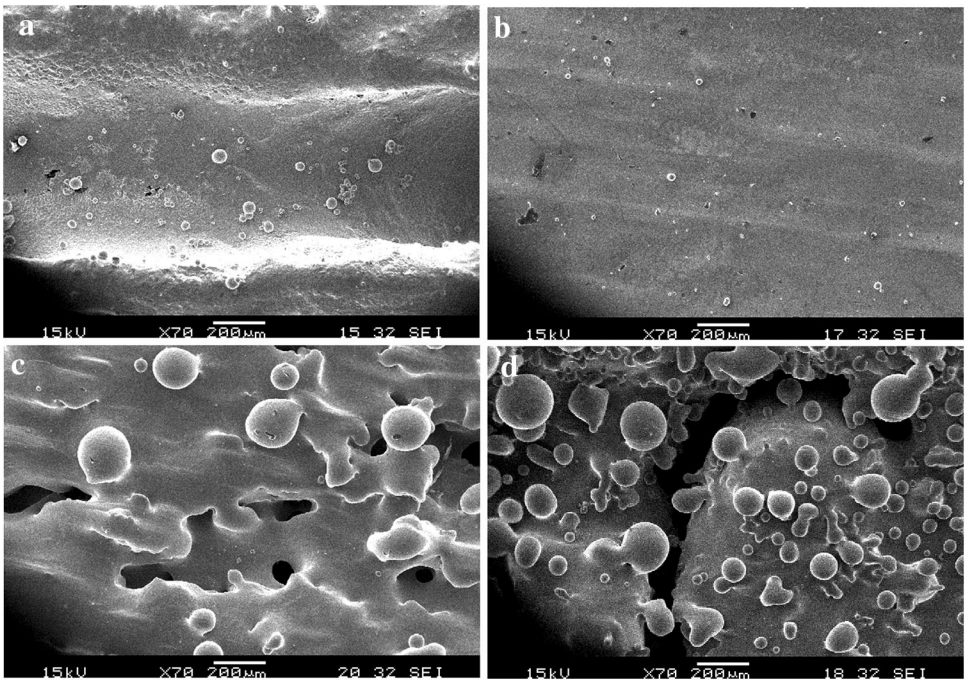

Fig. 2 SEM images of **a** P15–60, **b** P25-60, **c** P40–60 and **d** P60–60 samples produced after S2. A constant E magnitude of 16.67 J/m was used throughout S2

between the various states of the material during laser scanning.

According to the research by Tolochko et al., the materials in the powder form tend to have a much higher laser absorptivity than in the dense form [27]. This is because the laser radiation is able to penetrate through the inter-particle pores and causes interaction with the underlying powder particles. The absorption of the radiation by the pores may sometimes approach the absorption of a blackbody. Since E values of 11.11 and 16.67 J/m have larger magnitudes, the high laser absorptivity and low heat conductivity of the powder particles shown in Fig. 3a contributed to a greater degree of melting during S1. Thus, the presence of the pores will decrease significantly during the melting phase and the P40 and P60 samples will have a high density. Consequently, as presented in Fig. 3c, their low laser absorptivity reduces the amount of energy absorbed during S2. Moreover, their high heat conductivity

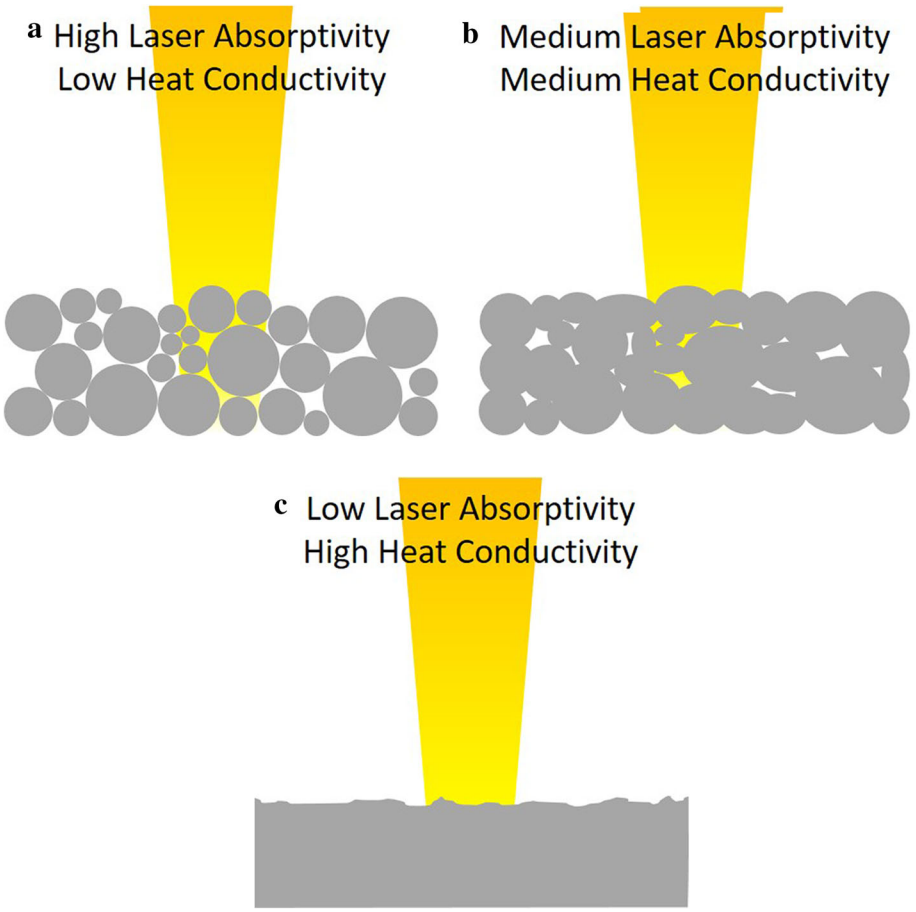

Fig. 3 Schematic of differences in laser absorptivity and heat conductivity: **a** powder particles, **b** P25, **c** P40 and P60 samples

assisted in transferring most of the absorbed energy away. Hence, P40 and P60 samples will experience a lower temperature during S2, resulting in a poor wetting condition and the formations of porosity and balling effect [29, 30].

However, the P25 samples produced were less dense when E decreases to 6.94 J/m. Subsequently, these samples experienced a higher temperature than P40 and P60 samples during S2. This decreases the viscosity of the molten pool, lowers the wetting angle and reduces the surface tension [28, 29, 31]. These phenomena then contributed to the efficient densification of the samples without the occurrence of the balling effect. Nonetheless, further reduction of E to 4.17 J/m produces a minimum amount of melting as presented in Fig. 1a. Thus, P15 samples have a high laser absorptivity and a low heat conductivity. As a result, they experienced a higher temperature at a localised point during S2. This generates a more pronounced temperature gradient, leading to high thermal stresses and eventually causes the warping effect [32].

In general, samples with seemingly excellent properties were produced by optimising the laser power. The different magnitudes used have a huge influence on the laser absorptivity and heat conductivity of the samples fabricated after S1. These two characteristics will then affect the final properties of the SLM NiTi parts produced after S2. The apparent superior quality of the P25–60 samples will be characterised and verified in the next section.

Characterisation of Optimised Samples

Four P25–60 square samples and NiTi powder were subjected to DSC testing. Their DSC curves and transformation temperatures were compared and presented in Fig. 4 and Table 1, respectively. The average transformation temperatures of P25–60 samples are similar to that of NiTi powder, except for the A_s temperature. However, this difference can be considered negligible. This is the result of the compositional sensitivity of NiTi, where its transformation temperatures are significantly influenced by its chemical composition [25, 33, 34]. Moreover, the P25–60 samples have demonstrated high repeatability as indicated by the small deviations in their transformation temperatures. They have also exhibited similar phase transformation characteristics as the given NiTi powder, where double peaks were observed in their DSC curves shown in Fig. 4. In addition, previous works have also reported the same

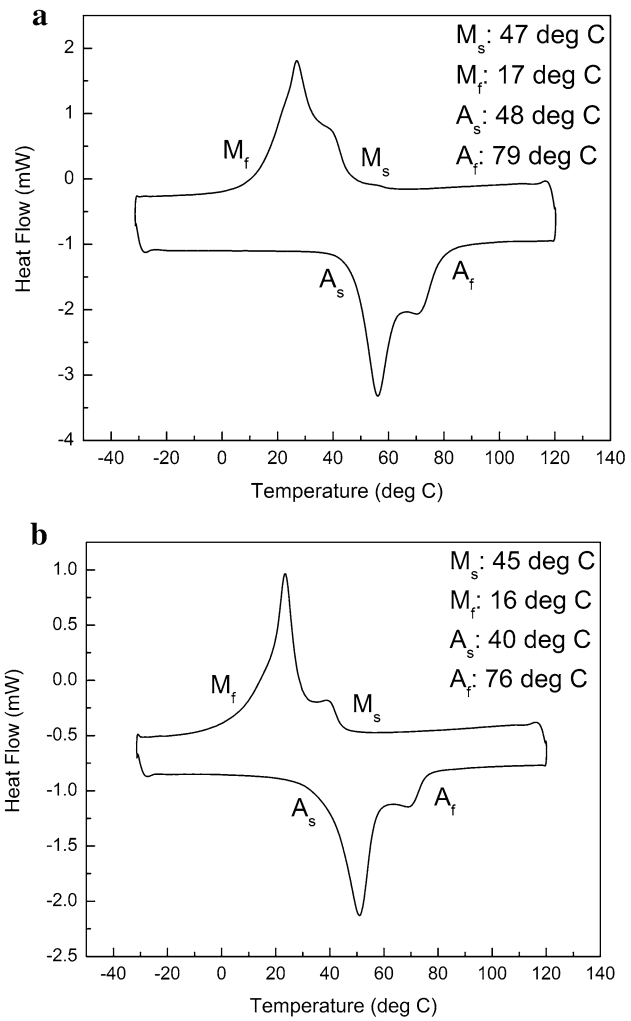

Fig. 4 DSC curves of **a** NiTi powder and **b** one P25–60 sample tested

Table 1 Average transformation temperatures of four P25–60 samples and NiTi powder tested

	Transformation temperatures			
	M_s (°C)	M_f (°C)	A_s (°C)	A_f (°C)
NiTi powder	47	17	48	79
P25–60 samples	45 ± 0	15 ± 1	40 ± 1	76 ± 0

phenomenon shown by the NiTi powder [35, 36]. One possible explanation was proposed by Mentz et al. [35]. They stated that "the NiTi powders considered here were formed in a rapid process and thus the resulting material states are far from being in thermodynamic equilibrium. Decomposition processes or shrinkage related stresses may well affect the transformation behaviour." However, more studies are needed to understand such occurrence. Additionally, the ability of the produced samples to retain that second peak suggests the potential to conserve the properties of the provided raw materials even after the SLM fabrication.

The next important characterisation test would be to determine the shape-memory responses of the P25–60 samples. This is done by subjecting the four P25–60 long strip samples to tensile test. Compression test is not conducted as it ignores the effect of porosity. High porosity samples tend to fracture easily under tension load than under compressive load. The presence of the pores can contribute to stress concentrations when under tension and causes failure. Furthermore, a sample that demonstrates a high magnitude of shape recovery after compression does not always translate into a high shape recovery upon tensile load. The sample must be of a decent quality in order to withstand the tensile stress without failure. Thus, the determination of shape recovery property under tension load is an essential experiment for the SLM NiTi SMA. It evaluates the combined quality of the sample including porosities, ductility, transformation characteristics and most importantly SME.

Figure 5a illustrates the testing procedure via the stress–strain–temperature curve of one sample tested. Figure 5b, c, d presents the corresponding stress–strain curve, strain–temperature and its derivative curve, respectively. The derivative curve was plotted to determine the temperatures at which the shape recovery begins and finishes. Table 2 presents the average strain readings. The maximum strain refers to the strain that the sample is deformed to before unloading. The residual strain indicates the strain exhibited by the sample after unloading. The transformation strain is the strain of shape recovery while the permanent strain denotes the remaining strain after shape recovery completed. According to Table 2, the average transformation strain is 4.61%. It was calculated based on the results of four samples (4.78, 4.18, 4.37 and 5.11%). This result is comparable to the transformation strain of 6% exhibited by the conventionally produced NiTi [6]. Furthermore, the result also presented a great improvement in the transformation strain as compared to the prior work of 0.5% transformation strain [20]. For comparison purposes, four P60 (single scan) long strip samples were fabricated and tensile loaded as well. However, none of the samples was able to deform beyond the 6% strain. The force–strain curve and micrograph of the best P60 sample tested are shown in Fig. 6. The results suggested that the P60 sample experienced fractures at multiple points before failing ultimately at 6% strain. It also demonstrated the significance of introducing repetitive scanning to enhance the properties of the SLM NiTi samples produced.

The permanent strains presented in Table 2 indicate incomplete shape recovery. It is well known that the SME is not perfect [7, 37–40]. The generation of the permanent

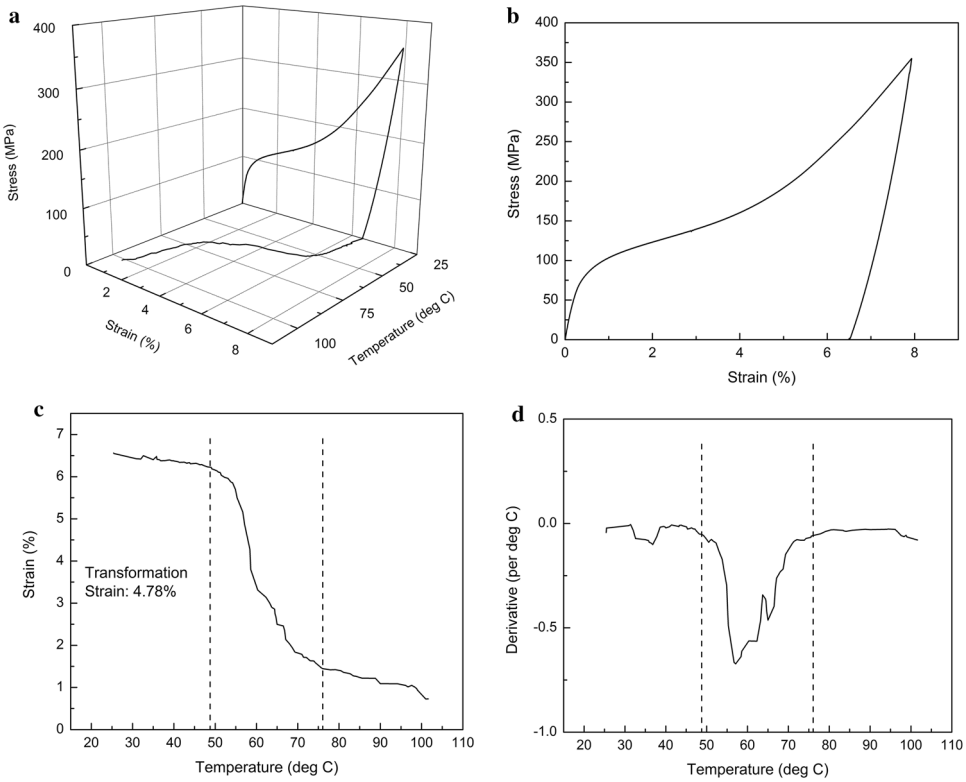

Fig. 5 The **a** stress–strain–temperature curve of one P25–60 sample tested. The corresponding **b** stress–strain curve, **c** strain–temperature curve and **d** strain–temperature derivative curve are presented

Table 2 Average strains from four P25-60 samples tested

Maximum strain (%)	7.94 ± 0.01
Residual strain (%)	6.50 ± 0.09
Transformation strain (%)	4.61 ± 0.36
Permanent strain (%)	1.49 ± 0.21
$\frac{\text{Transformation Strain}}{\text{Residual Strain}}$	0.71 ± 0.05

strain is a consequence of the formation of dislocations and specific martensite variants during tensile loading [37, 39–41]. An interesting observation reported by Ortega et al. [38] was the effect of alloy composition on the shape recovery magnitude in cast NiTi alloys. They attributed the better shape recovery properties in cast NiTi alloy to the formation of nanometre scale precipitates formed after mild ageing. This is worth of further investigation in the present SLM NiTi since SLM also involves a melting and solidification process.

The importance of the formation of nanoscale grains on the stress-induced phase transformation has also been reported in NiTi through Joule heating which limited the atomic diffusion due to very short heating time [42]. Both strengthening mechanisms of precipitation hardening [38, 39] and grain refinement aim to reduce irreversible plastic deformation and improve the functionality of NiTi. Another method would be the deformation of NiTi at intermediate temperature, for instance, 500 °C, to enhance its transformation strain and mechanical properties [43]. Besides, the incomplete detwinning of the presently optimised samples may also be related to the rapid solidification nature of the SLM process. Internal stress field might exist within the samples, leading to an adverse effect on the detwinning process [44]. Hence, the future research could include various post-processing treatments to improve the transformation strain. All the above mechanisms can be considered and explored in the future for improving the mechanical and thermomechanical properties of SLM NiTi alloys.

Conclusion

In this research, high-quality SLM NiTi samples were fabricated by introducing repetitive scanning. The laser powers adopted during the first scan and second scan correspond to 25 and 60 W while the laser scanning speed was kept constant at 3600 mm/s. The final properties of the produced SLM NiTi parts are heavily influenced by the differences in the laser absorptivity and heat conductivity of materials before and after the first scan. The advantages of adopting repetitive scanning and the excellent properties of the samples were confirmed by two results:

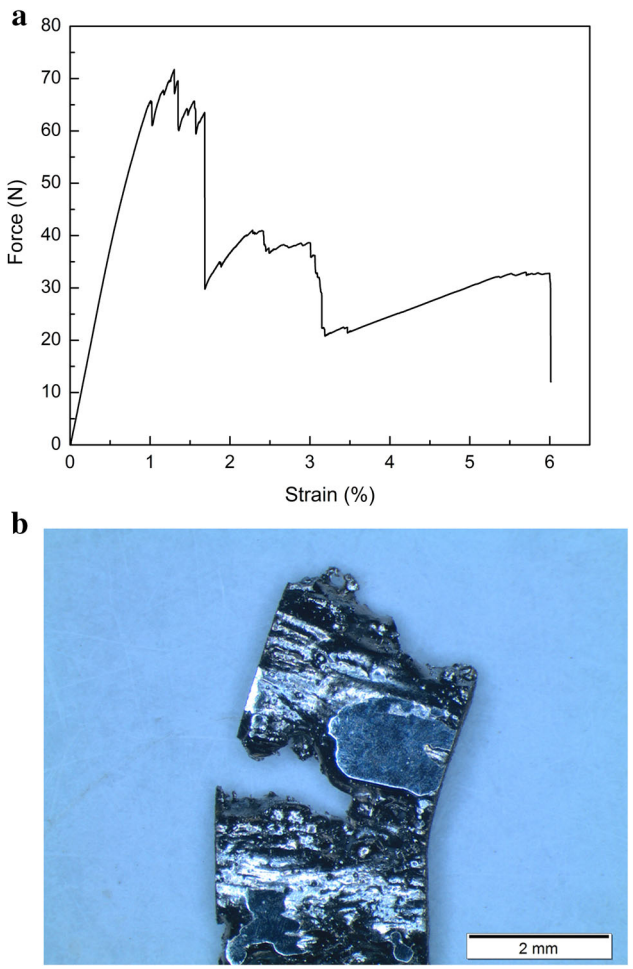

Fig. 6 **a** Force–strain curve and **b** micrograph of the best P60 (single scan) sample tested

1. The fabricated samples have demonstrated similar phase transformation characteristics as the given NiTi powder with high repeatability.
2. The produced samples are able to withstand tensile load and exhibit transformation strain as high as 5.11% with an average value of 4.61%, comparable to the conventionally made NiTi components.

These results suggested the potential of fabricating SLM NiTi with complex geometries and similar properties to the NiTi parts produced by conventional technologies.

Acknowledgements This work was funded by the School of Mechanical and Aerospace Engineering (MAE), Nanyang Technological University (NTU) through a Tier 1 project and by the Institute of Sports Research (NTU). The authors thank Prof. SF Yang for useful discussions.

References

1. Meier H, Haberland C, Frenzel J (2012) Structural and functional properties of NiTi shape memory alloys produced by selective laser melting. In: Bártolo (ed) Innovative developments in virtual and physical prototyping. Ruhr University Bochum, Bochum, pp 291–296
2. Elahinia MH, Hashemi M, Tabesh M, Bhaduri SB (2012) Manufacturing and processing of NiTi implants: a review. Prog Mater Sci 57:911–946
3. Dadbakhsh S, Speirs M, Kruth J-P, Schrooten J, Luyten J, Van Humbeeck J (2014) Effect of SLM parameters on transformation temperatures of shape memory nickel titanium parts. Adv Eng Mater 16:1140–1146
4. Kumar PK, Lagoudas DC (2008) Introduction to shape memory alloys. In: Lagoudas DC (ed) Shape memory alloys: modeling and engineering applications. Springer, Berlin, pp 1–51
5. Meier H, Haberland C, Frenzel J, Zarnetta R (2009) Selective laser melting of NiTi shape memory components. Presented at the advanced research in virtual and rapid prototyping, Leiria, Portugal
6. Hartl DJ, Lagoundas DC (2008) Thermomechanical characterization of shape memory alloy materials. In: Lagoundas DC (ed) Shape memory alloys: modeling and engineering applications. Springer, Berlin, pp 53–119
7. Haberland C, Elahinia M, Walker JM, Meier H, Frenzel J (2014) On the development of high quality NiTi shape memory and pseudoelastic parts by additive manufacturing. In: Smart materials and structures, vol 23, p 104002 (1–13)
8. Bormann T, Schumacher R, Muller B, Mertmann M, de Wild M (2012) Tailoring selective laser melting process parameters for NiTi implants. J Mater Eng Perform 21:2519–2524
9. Shishkovsky I, Yadroitsev I, Smurov I (2012) Direct selective laser melting of nitinol powder. Phys Procedia 39:447–454
10. Zhang B, Chen J, Coddet C (2013) Microstructure and transformation behavior of in situ shape memory alloys by selective laser melting Ti-Ni mixed powder. J Mater Sci Technol 29:863–867
11. Shishkovsky IV, Yadroitsev IA, Smurov IY (2013) Manufacturing three-dimensional nickel titanium articles using layer-by-layer laser-melting technology. Tech Phys Lett 39:1081–1084
12. Habijan T, Haberland C, Meier H, Frenzel J, Wittsiepe J, Wuwer C et al (2013) The biocompatibility of dense and porous nickel–titanium produced by selective laser melting. Mater Sci Eng, C 33:419–426
13. Dadbakhsh S, Speirs M, Kruth J-P, Van Humbeeck J (2015) Influence of SLM on shape memory and compression behaviour of NiTi scaffolds. CIRP Ann Manufac Technol 64:209–212
14. Bormann T, Müller B, Schinhammer M, Kessler A, Thalmann P, de Wild M (2014) Microstructure of selective laser melted nickel–titanium. In: Materials characterization, vol 94, pp 189–202
15. Clare AT, Chalker PR, Davies S, Sutcliffe CJ, Tsopanos S (2008) Selective laser melting of high aspect ratio 3D nickel-titanium structures two way trained for MEMS applications. Int J Mech Mater Des 4:181–187
16. Speirs M, Wang X, Baelen SV, Ahadi A, Dadbakhsh S, Kruth J-P et al (2016) On the transformation behavior of NiTi shape-memory alloy produced by SLM. Shape Mem Superelast 2:310–316
17. Dadbakhsh S, Vrancken B, Kruth J-P, Luyten J, Van Humbeeck J (2016) Texture and anisotropy in selective laser melting of NiTi alloy. Mater Sci Eng, A 650:225–232
18. Khoo ZX, Ong C, Liu Y, Chua CK, Leong KF, Yang SF (2016) Selective laser melting of nickel titanium shape memory alloy. In 2nd international conference on progress in additive

manufacturing, Nanyang Executive Centre, Nanyang Technological University, Singapore, 16–19 May 2016, pp 451–456
19. Khoo ZX, Lim YL, Liu Y, Chua CK (2016) Effect of hatch distance on selective laser melting of nickel titanium shape memory alloy. In: 2nd international conference in sports science & technology, Nanyang Executive Centre, Nanyang Technological University, Singapore, 12–13 Dec 2016, pp 98–101
20. Khoo ZX, Teoh JEM, Liu Y, Chua CK, Yang S, An J et al (2015) 3D printing of smart materials: a review on recent progresses in 4D printing. Virtual Phys Prototyp 10:103–122
21. Zhu HH, Fuh JYH, Lu L (2005) Microstructural evolution in direct laser sintering of Cu-based metal powder. Rapid Prototyp J 11:74–81
22. Khoo ZX, Low ZH, Liu Y, Chua CK, An J, Leong KF (2017) Repetitive laser scanning and shape recovery of SLM NiTi shape memory alloy. Submitted to Materials Letters
23. Yaws CL (2011) Chapter 66 Ni—nickel. In: Yaws handbook of properties of the chemical elements. Konvel, Norwich, pp 271–274
24. Yaws CL (2011) Chapter 103 Ti—titanium. In: Yaws handbook of properties of the chemical elements. Knovel, Norwich, pp 420–424
25. Miyazaki S, Kim HY (2011) Basic characteristics of titanium-nickel (Ti-Ni)-based and titanium-niobium (Ti-Nb)-based alloys. In: Yamauchi K, Ohkata I, Tsuchiya K, Miyazaki S (eds) Shape memory and superelastic alloys—technologies and applications. Woodhead Publishing Limited, Sawston, pp 15–42
26. Gu D, Shen Y (2009) Balling phenomena in direct laser sintering of stainless steel powder: metallurgical mechanisms and control methods. Mater Des 30:2903–2910
27. Tolochko NK, Laoui T, Khlopkov YV, Mozzharov SE, Titov VI, Ignatiev MB (2000) Absorptance of powder materials suitable for laser sintering. Rapid Prototyp J 6:155–160
28. Yadroitsev I, Bertrand P, Smurov I (2007) Parametric analysis of the selective laser melting process. Appl Surf Sci 253:8064–8069
29. Olakanmi EO, Cochrane RF, Dalgarno KW (2015) A review on selective laser sintering/melting (SLS/SLM) of aluminium alloy powders: processing, microstructure, and properties. Prog Mater Sci 74:401–477
30. Morgan R, Sutcliffe CJ, O'Neill W (2004) Density analysis of direct metal laser re-melted 316L stainless steel cubic primitives. J Mater Sci 39:1195–1205
31. Simchi A, Pohl H (2003) Effects of laser sintering processing parameters on the microstructure and densification of iron powder. Mater Sci Eng, A 359:119–128
32. Pohl H, Simchi A, Issa M, Dias HC (2001) Thermal stresses in direct metal laser sintering. In: Solid freeform fabrication symposium, University of Texas, Austin, pp 366–372
33. Frenzel J, George EP, Dlouhy A, Somsen C, Wagner MF-X, Eggeler G (2010) Influence of Ni on martensitic phase transformations in NiTi shape memory alloys. Acta Mater 58:3444–3458
34. Bhagyaraj J, Ramaiah KV, Saikrishna CN, Bhaumik SK, Gouthama (2013) Behaviour and effect of Ti2Ni phase during processing of NiTi shape memory alloy wire from cast ingot. J Alloys Compd 581:344–351
35. Mentz J, Frenzel J, Wagner MF-X, Neuking K, Eggeler G, Buchkremer HP et al (2008) Powder metallurgical processing of NiTi shape memory alloys with elevated transformation temperatures. Mater Sci Eng, A 491:270–278
36. Bansiddhi A, Dunand DC (2007) Shape-memory NiTi foams produced by solid-state replication with NaF. Intermetallics 15:1612–1622
37. Eggeler G, Hornbogen E, Yawny A, Heckmann A, Wagner M (2004) Structural and functional fatigue of NiTi shape memory alloys. Mater Sci Eng, A 378:24–33
38. Ortega AM, Tyber J, Frick CP, Gall K, Maier HJ (2005) Cast NiTi shape-memory alloys. Adv Eng Mater 7:492–507
39. Miyazaki S, Imai T, Igo Y, Otsuka K (1986) Effect of cyclic deformation on the pseudoelasticity characteristics of Ti-Ni alloys. Metall Trans A 17:115–120
40. Paradis A, Terriault P, Brailovski V (2009) Modeling of residual strain accumulation of NiTi shape memory alloys under uniaxial cyclic loading. Comput Mater Sci 47:373–383
41. Liu Y, Xie Z (2007) Detwinning in shape memory alloy. In: Reece PL (ed) Progress in smart materials and structures. Nova Science Publishers, New York, pp 29–65
42. Delville R, Malard B, Pilch J, Sittner P, Schryvers D (2010) Microstructure changes during non-conventional heat treatment of thin Ni–Ti wires by pulsed electric current studied by transmission electron microscopy. Acta Mater 58:4503–4515
43. Ataei M, Zarei-Hanzaki A, Shamsolhodaei A (2017) Shape memory response and mechanical properties of warm deformed NiTi intermetallic alloy. Mater Sci Eng, A 680:291–296
44. Liu Y, Humbeeck JV, Stalmans R, Delaey L (1997) Some aspects of the properties of NiTi shape memory alloy. J Alloys Compd 247:115–121